ORIGINAL ARTICLE

Green electrochemical polishing of EBM Ti6Al4V samples with preliminary fatigue results

Annalisa Acquesta[1] · Tullio Monetta[1] · Stefania Franchitti[2] · Rosario Borrelli[2] · Antonio Viscusi[1] · Alessia Serena Perna[1] · Francesco Penta[3] · Luca Esposito[1] · Luigi Carrino[1]

Abstract

Additive manufacturing technologies have several well-known advantages; however, the surface quality of the printed parts is poor, compromising the corrosion and mechanical properties. Thus, surface finishing treatments are necessary. The most post-processing treatments proposed in the literature are mechanical or chemical. The formers are contact techniques and cannot be suitable for complex geometry, while the latter use strong and dangerous reagents. This paper is aimed to investigate the effect of the electropolishing treatment, a contactless technique, using an eco-friendly electrolytic solution in reducing the roughness and improving the fatigue properties of Ti6Al4V specimens produced by electron beam melting technology. Several parameters affecting the effectiveness of the electropolishing treatment have been investigated, as interelectrode distance, stirring rate and duration time. An optimal combination of them allowed a uniform surface treatment and a significant roughness reduction (64% of Sa reduction for cylindrical specimens). Under sinusoidal loading conditions with a maximum stress of 378 MPa and a stress ratio equal to $R = 0.1$, the mean fatigue life of electropolished dog-bone specimens was 250% longer than that of as-built specimens.

Keywords Additive manufacturing · Electropolishing treatment · Roughness · Fatigue property · Eco-friendly treatment

1 Introduction

Additive manufacturing (AM) technologies have gained a growing academic and industrial interest in producing near-net-shape, complex and customisable components that cannot be fabricated with conventional manufacturing. The new technologies allow building a component from a CAD model by adding material layer-by-layer. The most AM-used methods are powder-based technologies in which a laser or an electron beam, melts or sinters powders. The latter can be uniformly spread on the building platform, as in selective laser melting (SLM) [1] or electron beam melting (EBM) [2], or can be blown out from nozzles, as in directed-energy deposition (DED) [3]. AM technologies used to produce complex-shaped titanium-based parts represent an attractive alternative to the conventional ones that involve a large amount of material waste, high cost, and long processing time. For example, the relatively high "buy-to-fly" ratio, defined as the ratio between the mass of raw material needed to produce a component and the final mass, is in the order of 25:1 for aircraft components made of titanium alloys using traditional processes. The AM technologies reduce the high buy-to-fly ratio to (3–12):1 [4]. Several studies have been carried out in the literature proving the potentiality of AM technologies, and different papers were published by the scientific community showing the advantages of layer-by-layer manufacturing methods [5]. However, some drawbacks can limit their applications; in fact, the AM techniques are characterised by functional constraints that would have to be overcome, such as manufacturing defects, high tensile residual stresses, and the printed components' surface quality [6]. These limits involve a detrimental effect on the mechanical performance and corrosion behaviour of the as-built parts, precluding their applications [7–9]. A critical issue is related to the fatigue performances of additively

✉ Annalisa Acquesta
  annalisa.acquesta@unina.it

1   Department of Chemical, Materials and Production Engineering, University of Naples Federico II, 80125 Naples, Italy

2   Italian Aerospace Research Centre, 81043 Capua, Italy

3   Department of Industrial Engineering, University of Naples Federico II, 80125 Naples, Italy

manufactured parts. Generally, lower fatigue strength and a larger scatter in the fatigue life of AM parts are ascribed to high surface roughness and manufacturing defects [10, 11]. Hu et al. [12] have characterised the manufacturing defects population by X-ray micro-computed tomography, which are essentially lacks fusion (LoF) and porosity. LoF arises from the incomplete melting between deposited layers. While porosity or voids commonly arise from pores in the particle feedstock, often containing trapped gases. The defects' nature, shape and position play a role in the fatigue durability of the AM part [13]. LoFs are generally larger and more irregularly shaped than porosity, making them more critical. In any case, surface defects were more critical than internal defects [14, 15]. The high surface roughness is due to some effects, such as rippling, stairstep, balling and partially or un-melted particles attached to the solidified part formed during the AM process. Thus, post-processing treatments are needed.

1.1 Post-processing treatments

To date, scientists have developed several surface post-processing treatments, and different techniques have been applied to enhance the surface characteristics of the additively manufactured components [16]. Mechanical or chemical treatments are the most used for these purposes. However, the former, as sandblasting or laser shot peening, can involve deformations or tensile state on the surface and cannot treat complex shape components, as shown by the authors [17]; the chemical ones are performed using highly polluting reagents [18]. Developing new methodologies capable of overcoming these issues and ensuring effective surface treatments is needed. In this scenario, a potential solution can be the new electrochemical polishing (EP) treatment generation [19]. Since its discovery, the EP treatment has been performed using strong acids, such as perchloric-acid acetic mixtures [20]. Due to explosions that occurred during its use, the perchloric acid has been partially supplied by a combination of concentrated acids, such as phosphoric and sulphuric ones. Therefore, the issues related to using acid baths in terms of handling and disposal are timely present. In addition, the EP treatment is usually performed at high or very low temperatures and high values of tension or current density, affecting the cost process [21].

1.2 Acid-free electropolishing treatment: state of the art

Few researchers are focused on investigating new acid-free electrolytes applying "normal conditions" regarding temperature and current density. In 2008, Tajima et al. [22] studied the EP treatment performed in a safe electrolytic solution composed of ethyl alcohol, isopropyl alcohol, aluminium

chloride and zinc chloride on two groups of CP titanium and its alloy, holding the temperature at 25, 30 and 35 °C but applying high current density values in the order of kA/cm². Kim et al. [23] investigated the effect of adding ethanol to an electropolishing solution ethylene glycol-based to treat a CP2 Ti sheet, performing the treatment at 20 °C and applying 20 V. Recently, some researchers have studied the possibility of applying EP treatment to additive manufacturing Ti6Al4V-based parts [24]. Urlea and Brailovski [25] used the classical acid-based EP process to reduce the roughness of SLM Ti6Al4V components characterised by variably oriented surfaces. The authors highlighted an evident influence of the building orientation adopted to fabricate the components. Benedetti et al. [26] investigated the mechanical properties and biocompatibility of SLM Ti6Al4V ELI cylindrical specimens built with a direction of 90° after different post-sintering treatments. They observed that the EP treatment improved fatigue behaviour by 14%. Wu et al. [27] studied the effect of the classical acid-based EP on corrosion and mechanical properties of Ti6Al4V tensile test specimens. They revealed a gradual improvement of the ultimate tensile stress and tensile elongation after the EP post-treatment. A wide passivity range was observed after the electropolishing treatment, although corrosion resistance was decreased for over-polished parts. Pyka et al. [28] applied a combination of chemical etching and electrochemical polishing to reduce the roughness of the lattice structure of SLM-produced Ti6Al4V, highlighting the need to optimise the treatment to reduce the roughness without decreasing the mechanical properties. Although the previous results seem to effectively reduce the parts' roughness and improve the mechanical properties of additively produced parts, very pollutant electrolytes are still used [24]. Therefore, the possibility of using low environmental impact materials has to be a priority.

1.3 Aims of the research

In this view, the present paper aims to show the results of EP treatment performed by using an eco-friendly electrolytic solution to significantly reduce the roughness and improve the mechanical properties of EBM-manufactured Ti6Al4V parts. For this purpose, cylindrical-shaped and dog-bone samples were printed and treated using electropolishing. Compared to dog-bone samples, the cylindrical typology was chosen due to the simpler geometry of specimens to be treated through EP for setting the process. The as-built and treated specimens were observed through the confocal microscope to analyse the surface roughness and morphology and set the proper EP treatment process parameters. Finally, a comparative fatigue analysis was carried out on dog-bone samples to assess the effects of the electrochemical treatment on the mechanical performances of the Ti6Al4V printed parts.

2 Materials and methods

2.1 Powder characterisation and parameters of the EBM process

Specimens used in this study were manufactured using Ti6Al4V plasma atomized powder with spherical morphology. The spherical shape contributes to improved flowability and, thus, ensures high build rates and part accuracy [29]. The powder flow rate measured according to ASTM B213 [30] was 25 s/50 g. According to ASTM B212 [31], the apparent density was 2.57 g/cm^3. As far as the particle size distribution is concerned, the percentage by mass of particle size in the range 45–106 μm was found equal to 93.6%, while most of the particles (62.1% of the mass) resulted in the range 53–75 μm. The powder's nominal chemical composition is reported by Franchitti et al. [11]. The electron beam melting system utilised in this study was the Arcam A2X with embedded EBM control version 3.2 software. This system allows solid parts to be directly manufactured from metal or alloy powder [32]. A standard Ti6Al4V build theme for a layer thickness of 50 μm was adopted. This build theme varies electron beam parameters in a controlled sequence throughout the build according to algorithms developed by the manufacturer to achieve fully dense as-built parts with consistent microstructure and properties. Since the algorithm is covered by copyright, beam current and beam speed time-dependent diagrams are hidden to the users. A line offset of 0.1 mm was set.

2.2 Specimens design and job preparation

Two types of specimens were realised (n° 24 cylindrical and n° 8 dog-bone-shaped samples). Cylindrical typology was chosen to set up the EP treatment, while the dog-bone shape was used to evaluate the effect of the EP process on the fatigue behaviour of EBM-printed Ti6Al4V parts. The samples' geometry and dimensions are shown in Fig. 1a and b. The samples' orientation and location in the build chamber were set using the Materialise Magics® software. In this work, a single grow orientation was considered. In particular, the samples, both cylindrical and dog-bone specimens, were manufactured in the z-direction growth orientations. All the specimens were scaled according to the ARCAM recommended scale factors to take into account the thermal shrinkage occurring after the melting. Wafer supports were needed in order to dissipate the heat generated by the electron beam. Circular supports were generated for each sample with a support length of 20 mm from the start plate and a line distance of 2 mm. The cylindrical specimens were manufactured in two identical jobs of n° 12 samples for a total of n° 24 samples. Instead, the dog-bone specimens were manufactured in a single job of n° 8 samples. Figure 1c shows the location, growth direction and wafer supports of the dog-bone specimens in the Materialise Magics environment.

2.3 Electropolishing treatment

In this investigation, a green electrolytic solution composed of ethylene glycol (> 99%), 0.5 M of NaCl and 10% vol. of ethanol was employed to treat as-built EBM additively manufactured parts, known to have a relatively high initial roughness [33]. All chemical reagents have been purchased from Merck. The EP treatment was carried out in a cell set-up, whose scheme is reported in Fig. 2. A magnetic stirrer was used to stir the solution, while a thermal bath was used to control and maintain the electrolytic solution at room temperature.
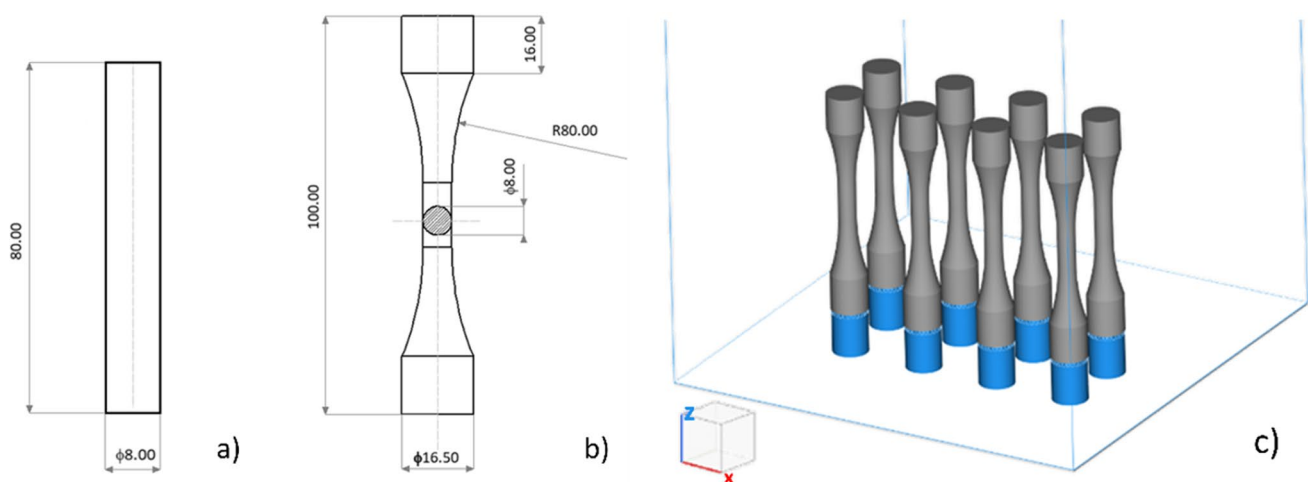
Fig. 1 **a** Geometry of the cylindrical specimens. **b** Geometry of the dog-bone specimens (dimensions in mm). **c** Job preparation for dog-bone specimens

Cylindrical and dog-bone-shaped samples were used as the anode. The EP treatment was performed by imposing a potential by a voltage generator (GEN 600–5.5, TDK-Lambda) and recording the current density value over time. Before and after the EP treatment, the samples were rinsed first in ethanol and after in water. Finally, they were dried with a compressed air stream.

As known from the literature, many parameters can influence the EP treatment [34], such as the anode–cathode distance [35], the solution stirring rate [36], the treatment time [37], and the solution temperature [22, 38] and others. The effects of the first three parameters have been investigated in detail following the experimental strategy based on the "one factor at a time" (OFAT) approach. The best condition has been identified sequentially (from time to time) through topographical, roughness and weight loss measurements. Firstly, the influence of the anode–cathode distance was investigated. A previous experimental campaign was performed on flat samples in Ti6Al4V produced by the additive

Fig. 2 Cell set-up used for the EP treatment

manufacturing EBM technique. It has allowed for obtaining a good level of electropolishing by stirring the electrolytic solution at a rate value of 1150 rpm for 60 min. The same conditions in terms of stirring rate and treatment time have been adopted for the electropolishing treatment to investigate the influence of inter-electrode distance.

On the other hand, the geometry of the present specimens was cylindrical; therefore, customised mesh cylindrical cathodes were additively manufactured using the same Ti6Al4V powders of the specimens. Due to the complex morphology of the specimen EBM-produced surface, the formation of a viscous layer on the anode electrode during the EP treatment and the fluid-dynamic phenomena related to the solution agitation [39], it was impossible to know a priori the proper interelectrode distance to obtain the smoothing of the surface. Thus, two cathodes with different diameters, $\Phi_1 = 35$ mm and $\Phi_2 = 65$ mm, schematically shown in Fig. 3, and an appropriate specimen gripping system to maintain the anode coaxial to the cathode were employed. Once fixed the most suitable interelectrode distance, the stirring rate influence has been investigated by setting its values at 0, 450 and 800 rpm while keeping the treatment time at 60 min to verify if a lower stirring rate could have a beneficial effect on the roughness reduction. Once the best stirring rate value was established, the influence of the EP treatment time was analysed to determine the minimum treatment time to reduce the surface roughness by at least 50%, so the treatment time was set at 15, 30 and 45 min. The material loss estimation was performed by weight measurements using an analytical balance (Sartorius 2001MP2) before and after the variations of stirring and time treatment parameters.

2.4 Topographical and roughness analyses

The surface roughness and morphology of both the as-built and treated cylindrical samples were analysed by confocal
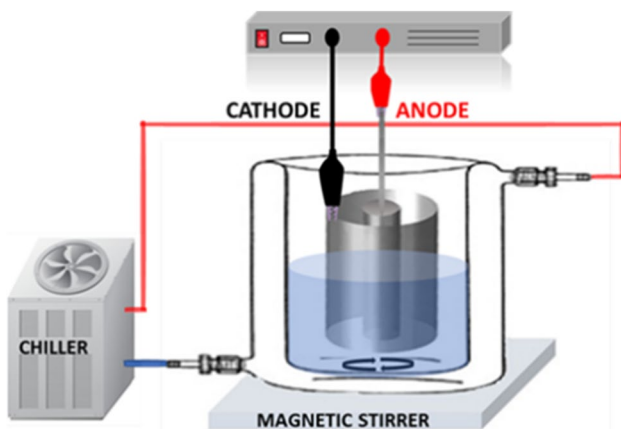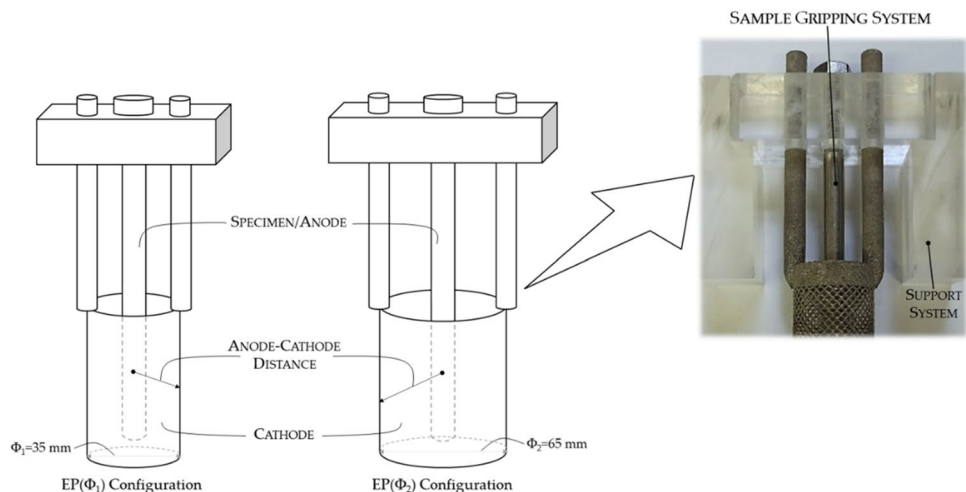
Fig. 3 Schematization of the experimental set-up used to analyse the effect of anode–cathode distance labelled as EP(Φ_1) and EP(Φ_2) configurations

microscope (Leica DCM3D Scan) to estimate the effectiveness of the EP process applied to EBM-manufactured Ti6Al4V parts. A scanning area equal to 3×3 mm was observed with an optical lens magnification equal to $\times 10$. The scan strategy was set in agreement with the illustrative sketch shown in Fig. 4.

The results have been exported to Leica Map® Software for data post-processing. Firstly, due to the cylindrical shape of the specimens, the acquired surface was levelled, and the form was removed. The waviness and roughness components of the surface analysed were separated through a Gauss filter, whose parameters have been chosen according to the ISO 16610 (2015) standard [40]. Topographical analyses and roughness parameters have been calculated using the same software, according to ISO 25178 standard [41].

Different surface parameters can be obtained from the roughness measurements; however, as proved in the literature [42], the most significant ones that effectively evaluate the EBM-printed components' surface morphology are as follows: S_a (arithmetical mean height); S_z (maximum height); S_q (root mean square height); S_{ku} (kurtosis as a measure of the sharpness of the roughness profile); S_{dq} (root mean square gradient); and S_{dr} (developed interfacial area ratio). Three different samples under the same process conditions were observed, and three different measurements per sample were performed for the repeatability of the results.

2.5 Fatigue testing

In general, the fatigue life of a component is influenced by several factors, such as the type of material, the manufacturing process, the surface finishing, as well as the size, orientation and type of defects [43]. Since it is technically impossible to control all these parameters, fatigue life is generally treated as a stochastic variable to which, for each level of stress, a certain probability of failure can be associated by statistical tools. Consequently, a statistical analysis of the fatigue behaviour of a material/product requires a significant number of tests. To obtain the Stress-Life (S–N) curve, the ASTM E739 standard [44] suggests a minimum number of 6 to 12 specimens and a good replication for each stress level. For this comparative and exploratory research, a total number of 8 dog-bone specimens for fatigue testing, compliant with the standard ASTM E466 [45], were prepared. After EBM manufacturing, four samples were tested under as-built conditions, and four specimens were EP-treated and then tested. Given the small number of samples, it was decided to compare treated and as-built samples at the same stress level to have good statistical repeatability. All specimens were fatigue tested under force-controlled conditions on a Zwick vibrophore Amsler HFP 250 with a 100 kN load cell capacity. The load consisted of a sinusoidal waveform with a maximum stress of 378 MPa and a stress ratio ($R = \sigma_{min} \backslash \sigma_{max}$) equal to 0.1. Tested samples were observed by a Zeiss stereo microscope to highlight the fracture surface morphology. The fatigue lives for the two sets were analysed under the classical assumption of lognormal distribution for the probability density function of the cycles to failure N, whose equation is

$$P_{df} = \frac{1}{\sigma \sqrt{2\pi}} e^{-\frac{1}{2}\left(\frac{\log(N)-\mu}{\sigma}\right)} \tag{1}$$

Fig. 4 Illustrative sketch of scan strategy used for confocal observations on cylindrical samples to set the EP process
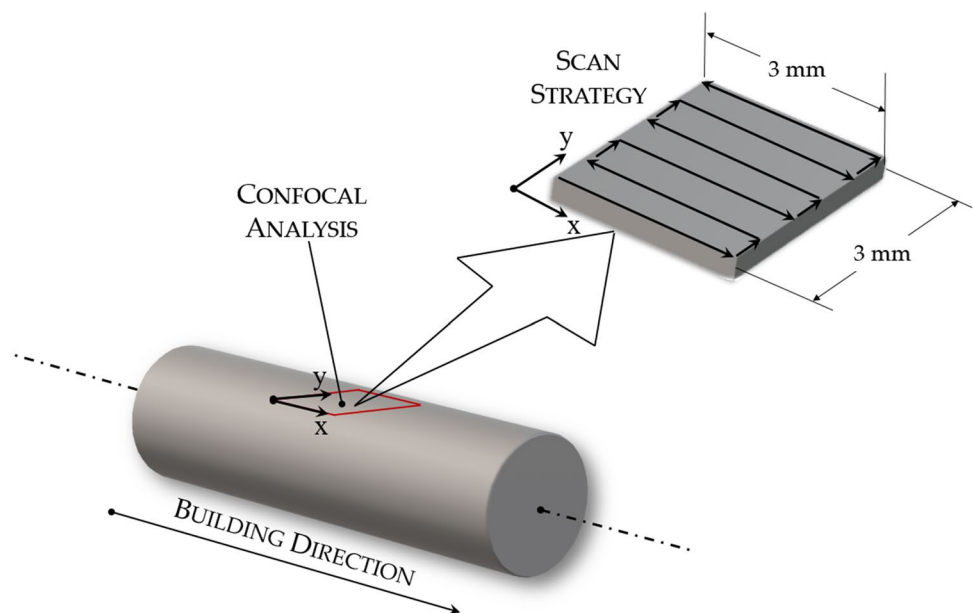
where parameter μ is the mean of the distribution, while σ is the standard deviation.

3 Results and discussion

In this section, firstly, the results from the green EP process will be presented. Then, the results obtained from the roughness analyses carried out on both the as-built and the EP-treated cylindrical samples are reported and discussed, focusing attention on the effects of the anode–cathode distance, the solution stirring rate and the treatment time. Afterwards, the comparative fatigue analysis outcomes on dog-bone samples are presented to assess the effects of the EP treatment on the mechanical performances of the Ti6Al4V printed parts.

3.1 Electropolishing process

Based on the Jacquet studies [46], recording the applied voltage and current density curve, it is possible to define the optimal conditions for EP treatment. These conditions occur when the current density reaches a constant value by increasing the applied potential. Unfortunately, the limiting current density plateau is not always easily identifiable, as demonstrated by several researchers reported by Acquesta and Monetta [24]. Indeed, many authors have defined the EP range based on preliminary experiments. Also, in this study, from the current density vs potential curve depicted in Fig. 5, it is possible to observe the lack of a typical current limiting plateau recorded for the classic acid-based electrolyte. However, based on the previous experimental campaign, in which the EP was performed between 15 and 20 V with poor results due to the too-low current densities recorded, a possible EP range was identified between 20 and 25 V, in which the current densities were slightly greater than those recorded in the previous range. Therefore, it was chosen to perform the EP treatment, in potentiostatic mode, at the highest value of the identified EP range (25 V) [20, 37].

The physical phenomena involved during EP treatment are very complex due to the speed with which they occur. It was possible to assume at the beginning of the process and apply a potential value higher than 10 V the dissolution of the natural oxide layer on the anodic surface, according to Fushimi [47]. The metals are well known to be covered by a natural air-formed oxide layer when exposed to the environment. It is possible to assume that also the as-built parts under this exam are covered by this oxide layer. Immediately after, a yellow viscous layer formation [46] is easily identifiable near the anodic surface. It could be the titanium tetrachloride ($TiCl_4$), as supposed by Kim et al. [23], which reported the possible chemical reactions enveloped during the treatment.

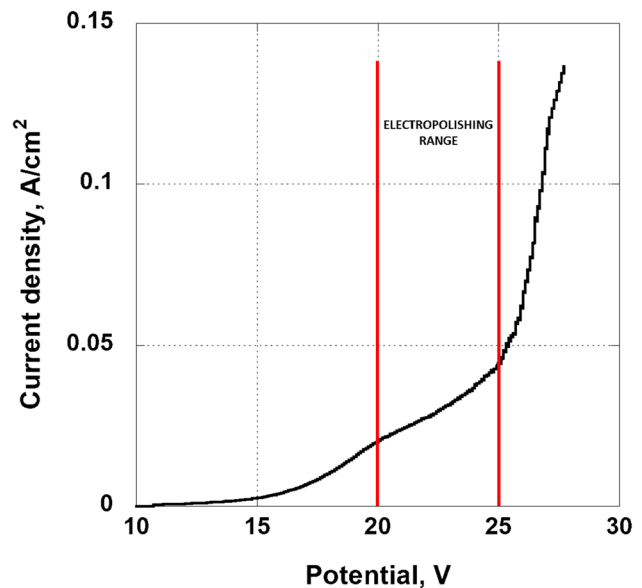**Fig. 5** Current density vs potential curve of the cylindrical sample

$$Ti \rightarrow Ti^{+4} + 4e^- \tag{2}$$

$$Ti^{+4} + Cl^- \rightarrow TiCl_4 \tag{3}$$

Although a very low oxygen amount is present in the electrolytic solution, due to the natural absorption of oxygen from the environment, a brown film is simultaneously formed on the anodic surface, suggesting the formation of a new oxide layer, as suggested by Fushimi et al. [37]

$$TiCl_4 + 2H_2O \rightarrow TiO_2 + 4H^+ + 4Cl^- \tag{4}$$
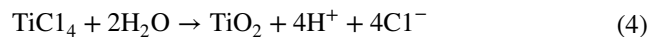
It was possible to presume the simultaneous formation of titanium ethanolate, according to the reaction:

$$4C_2H_6O + TiCl_4 \rightarrow C_8H_{20}O_4Ti + 4H^+ + 4Cl^- \tag{5}$$

The titanium ethanolate is soluble in organic solvents but hydrolyses readily, so it was possible to presume that it reacts with the shallow amount of water following the reaction:

$$C_8H_{20}O_4Ti + 2H_2O \rightarrow TiO_2 + 4C_2H_6O \tag{6}$$
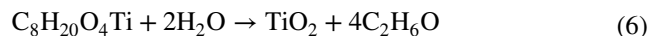
It involves the production of titanium oxide, but what matters is that it happens far from the anode electrode. The titanium oxide is a stable film and firmly adheres to the titanium substrate hindering its dissolution process. As a result, to have the maximum efficiency of the EP treatment, it is essential to contain this oxide layer formation, reducing the oxygen amount in the electrolytic solution, adding a compound with lower polarity than water or improving the stirring rate. Further, a defined stirring rate allowed for obtaining a significant roughness reduction of the as-built parts, as shown in the following paragraphs.

Therefore, the chemical analyses in progress will be helpful in understanding which chemical reactions are involved in the process.

3.2 Topographical and roughness measurements

This section presents the results obtained from topographical and roughness analyses through confocal microscopy.

3.3 Influence of anode–cathode distance

The beneficial effects of the reduced anode–cathode distance are visible from the topography of the as-built and EP specimens treated using the two kinds of cathodes (Φ_1 and Φ_2) depicted in Fig. 6.

The contour colour scale from Fig. 6 shows that the cathode typologies used during the EP process make the surface smoother than the as-built case. Take note that the images' colour scale is different to better visualise the different surface morphologies of the investigated samples. However, the smoothing capacity of the EP treatment has been quantified through the surface parameters from roughness measurements results reported in Table 1.

It may be noticed that relatively high surface roughness values characterise the as-built specimen, as proved in literature for EBM-printed components [48]; moreover, the relatively high values of both Kurtosis, S_{ku}, and root mean square gradient, S_{dq}, parameters indicate a very rough surface with sharp peaks. An interesting parameter is S_{dr} which is equal to 144% in the case analysed. That means an additional surface area (12.96 mm^2), due to the pronounced roughness, compared to the planar definition area (9 mm^2). Reduced surface roughness parameters were found for both EP specimens reported in Table 1. In particular, the best result was obtained for the EP(Φ_1) configuration characterised by a smaller distance between the anode and the cathode. More in detail, it can be seen that a reduction of S_a of about 64% was estimated with the more levelled treated surface (see the reduced S_{dq} value for EP(Φ_1)) characterised by more rounded peaks. In this case, the developed area is equal to 15.7%, lower than the value measured for EP(Φ_2) and as-built specimens. The main result of this analysis is that the reduced distance between the anode and cathode during the EP process has beneficial effects on the roughness: the smaller cathode ($\Phi_1 = 35$ mm) is enough to promote the effects of the electropolishing treatment, and thus it has been adopted for the following analysis.

3.4 Influence of stirring rate

The influence of the solution stirring rate was analysed based on the previous results. In Fig. 7, the surface topography of the EP specimens treated by varying the stirring solution rate is reported.

By looking at the contour colour scale in Fig. 7, it can be seen that all the surfaces after the EP treatment appear
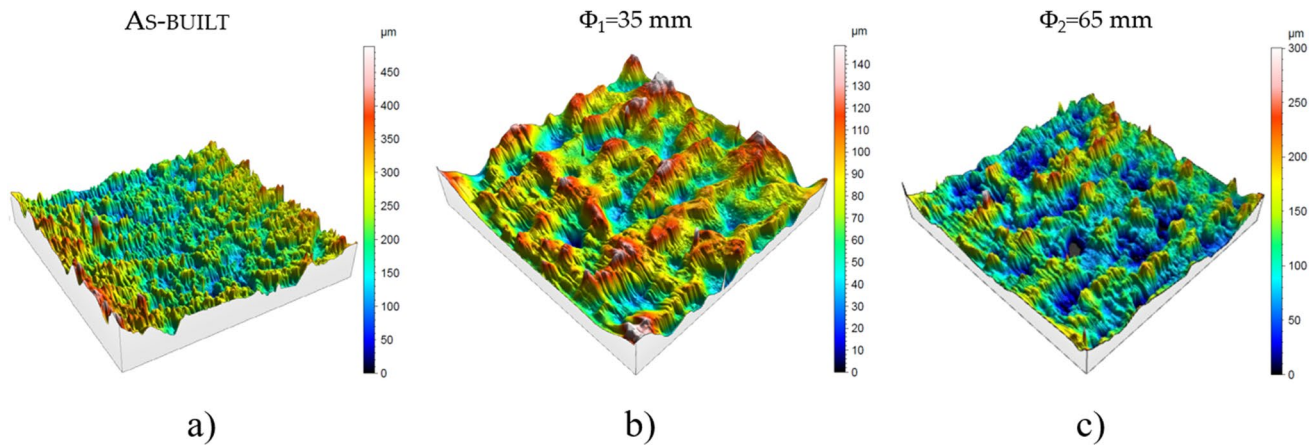
Fig. 6 Surface topography of metal surface: **a** as-built specimen, **b** EP-treated specimen with $\Phi_1 = 35$ mm, **c** EP-treated specimen with $\Phi_2 = 65$ mm. For both the treated specimens: stirring rate $= 1150$ rpm, treatment time $= 60$ min

Table 1 Surface parameters from roughness measurements for as-built specimen and EP-treated specimens with $\Phi_1 = 35$ mm and $\Phi_2 = 65$ mm

	S_a [μm]	S_z [μm]	S_q [μm]	S_{ku} [−]	S_{dq} [−]	S_{dr} [%]
As-built	50.9 ± 5.6	489 ± 46.9	64.6 ± 5.5	3.38 ± 0.4	3.45 ± 0.6	144 ± 15.2
EP(Φ_1)	18.3 ± 0.8	148 ± 7.7	22.8 ± 1.2	2.85 ± 0.2	0.89 ± 0.1	15.7 ± 0.8
EP(Φ_2)	35.6 ± 1.8	300 ± 13.9	44.4 ± 2.4	2.99 ± 0.3	2.86 ± 0.2	93.1 ± 5.1

smoother than those as-built specimens (Fig. 6a); moreover, the best result is reached when the solution stirring rate is equal to 1150 rpm (Fig. 7d). More details on the effects of this EP process parameter can be found by considering the data reported in Table 2.

It can be noticed that all the surface roughness parameters are smaller than the as-built ones. On the other hand, moving from 0 to 450 rpm, the treatment effectiveness slowly reduces (namely, the surface parameters increase), and this reduction seems to be more prominent, moving towards 800 rpm. However, a higher stirring rate reverses the direction, recording the lowest roughness value. This effect could be due to many causes. They can be related to (i) the viscous layer presence and its thickness, which certainly change with the stirring rate; (ii) the oxygen dissolution

through the viscous layer, from which the surface passivation depends; (iii) the complex fluid-dynamic phenomena concerning diffusive and convective fluxes of dissolved and formed substances; and (iv) the modification morphology surface, as exhibited by specimens treated fixing a stirring rate of 800 rpm. Its S_{ku} value was higher than 26% of the as-built specimen. This means that sharper peaks characterise the surface. Additional analyses are needed to investigate the aspects above-mentioned.

3.5 Influence of duration time treatment

The suitable EP conditions derived from the above analyses ($\Phi_1 = 35$ mm, rpm $= 1150$) were used to analyse the influence of the EP treatment time on the topography and
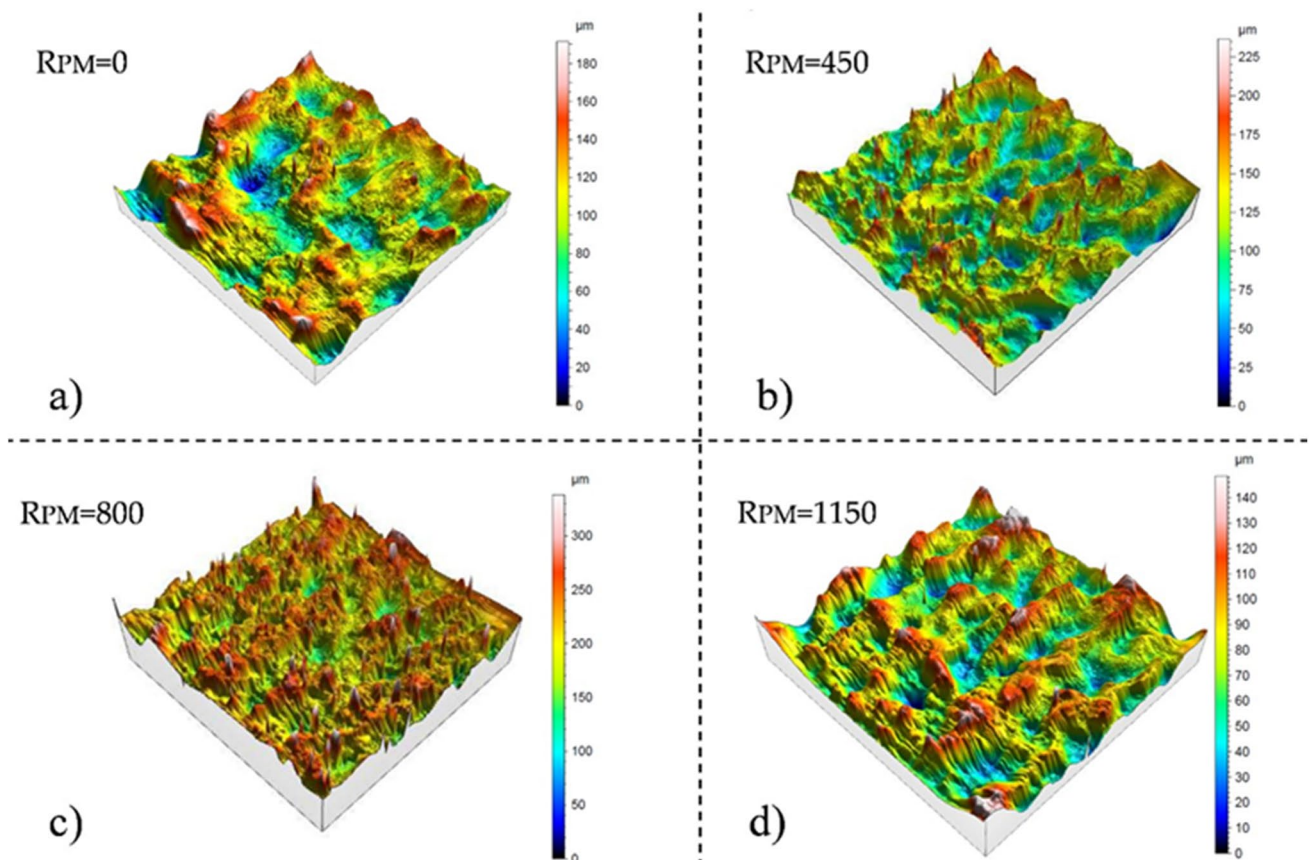

Fig. 7 Surface topography of EP specimens treated by varying the solution stirring rate: **a** rpm $= 0$, **b** rpm $= 450$, **c** rpm $= 800$, **d** rpm $= 1150$

Table 2 Surface parameters from roughness measurements by varying the solution stirring rate

	S_a [µm]	S_z [µm]	S_q [µm]	S_{ku} [−]	S_{dq} [−]	S_{dr} [%]
As-built	50.9 ± 5.6	489 ± 46.9	64.6 ± 5.5	3.38 ± 0.4	3.45 ± 0.6	144 ± 15.2
Rpm $= 0$	22.0 ± 0.9	191 ± 8.5	27.7 ± 2.1	2.96 ± 0.3	1.10 ± 0.1	18.8 ± 0.9
Rpm $= 450$	23.9 ± 1.1	237 ± 12.6	28.4 ± 1.7	3.25 ± 0.5	1.97 ± 0.3	44.6 ± 2.3
Rpm $= 800$	27.1 ± 1.7	338 ± 16.4	33.7 ± 1.9	4.29 ± 0.6	3.05 ± 0.5	77.5 ± 3.3
Rpm $= 1150$	18.3 ± 0.8	148 ± 7.7	22.8 ± 1.2	2.85 ± 0.2	0.89 ± 0.1	15.7 ± 0.8

surface roughness of the 3D-printed specimens. In particular, lower values than 60 min were considered by stopping the EP process after 15, 30 and 45 min. The topographical results obtained from the confocal microscopy are reported in Fig. 8.

By observing the surface topography and the contour colour scale of Fig. 8, it is clear that with the increase of the treatment time, the surface of the metallic specimens becomes smoother with more rounded and less sharp peaks. However, the smoothing capacity of the treatment was quantified through the surface parameters from the roughness measurements reported in Table 3.

From the data reported in Table 3, a slight reduction of the surface roughness can be seen moving from 15 to 30 min. More improvement was observed when the treatment time was set to 45 min (S_a reduced by about 17% compared to 30 min) or 60 min (S_a reduced furtherly by about

18% compared to 45 min). The results in Table 3 prove that the minimum time to obtain a roughness reduction of 50% is 15 min. On the other hand, a treatment duration of 60 min allowed to obtain a roughness reduction of about 64%.

3.6 Weight loss measurements

The weight loss measurements have confirmed the roughness results. The trends are shown in Fig. 9.

Regarding the stirring rate influence, it can be seen from Fig. 9a that the lack of agitation involves the highest weight loss due to the excessive attack on the free surface of the specimen; this phenomenon allows for obtaining the tungsten tips [49]. The weight loss is reduced, increasing the stirring rate, and reaching the lowest value for a stirring rate of 1150 rpm, due to a more homogeneous and contained dissolution process performed at current density
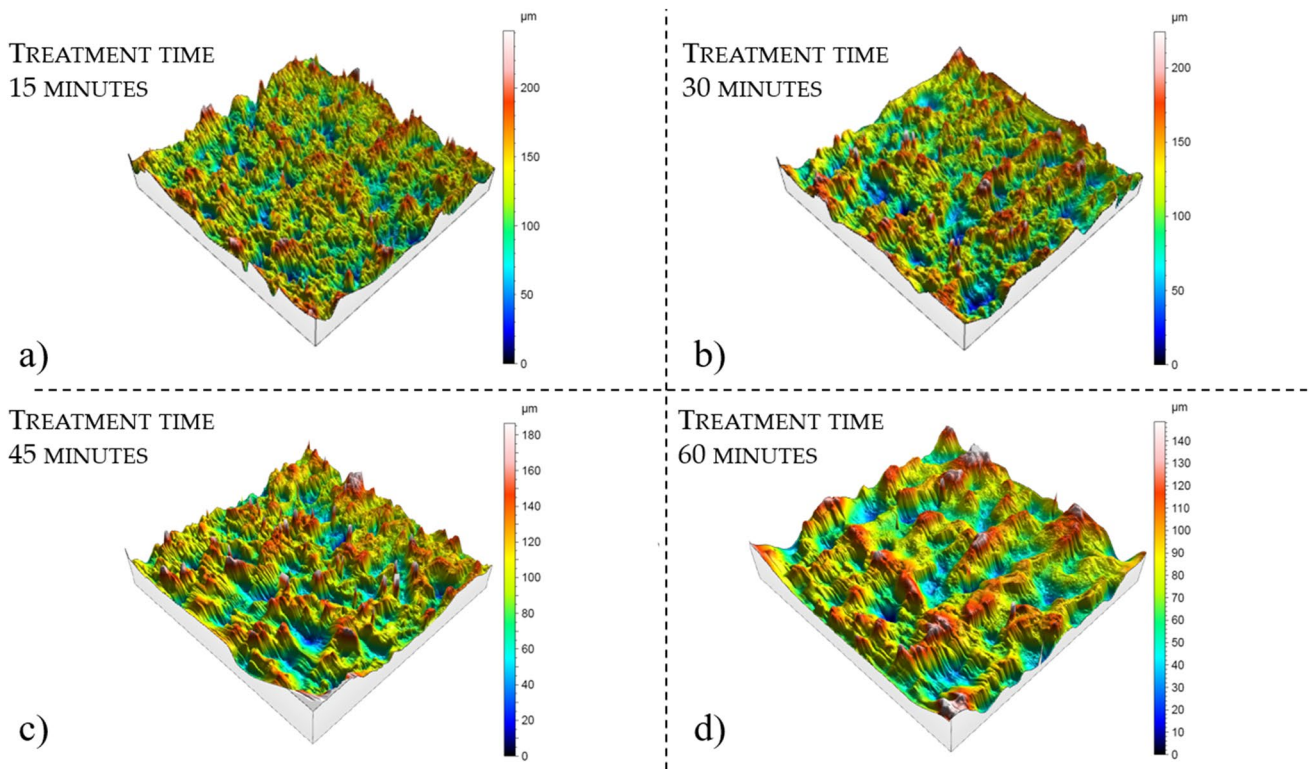

Fig. 8 Surface topography of metal surface for different treatment times: **a** 15 min, **b** 30 min, **c** 45 min, **d** 60 min

Table 3 Surface parameters from roughness measurements for different treatment times

| Treat. time [min]	S_a [µm]	S_z [µm]	S_q [µm]	S_{ku} [−]	S_{dq} [−]	S_{dr} [%]
0 (As-built)	50.9 ± 5.6	489 ± 46.9	64.6 ± 5.5	3.38 ± 0.4	3.45 ± 0.6	144 ± 15.2
15	27.5 ± 1.8	241 ± 13.2	34.6 ± 2.6	2.93 ± 0.3	2.82 ± 0.2	106 ± 5.7
30	27.3 ± 2.1	224 ± 12.0	34.4 ± 2.1	2.96 ± 0.2	2.29 ± 0.3	66.7 ± 4.1
45	22.5 ± 1.3	186 ± 9.4	28.5 ± 1.7	3.39 ± 0.8	1.78 ± 0.2	40.1 ± 2.4
60	18.3 ± 0.8	148 ± 7.7	22.8 ± 1.2	2.85 ± 0.2	0.89 ± 0.1	15.7 ± 0.8

values lower than recorded without agitation. Concerning the treatment time influence, as expected, longer treatment time leads to higher weight loss (Fig. 9b). Although a long treatment time may suggest a substantial weight loss, the material reduction after 60 min is 4.2%. This relatively low value of material loss compared to the high value of roughness reduction leads the authors to consider this time the best condition for an effective EP treatment.

In conclusion, based on the above results, a cathode with a diameter of 35 mm, a stirring rate of 1150 rpm, a treatment time of 60 min, and a potential of 25 V are the parameters' values adopted to polish the dog-bone specimens before being mechanically tested. A representative picture of dog-bone specimens before and after the EP treatment is shown in Fig. 10.

3.7 Fatigue results

The dog-bone samples for fatigue have been grouped in two sets labelled as (i) Z-as built, for post-printing status specimens; (ii) Z-EP, for electropolished specimens. The electropolished samples always showed longer fatigue lives than the as-built samples. The experimental cycles to failure are summarised in Table 4, where for each set, the values of the mean and standard deviation of the logarithmic values of the cycles to failure are also reported.
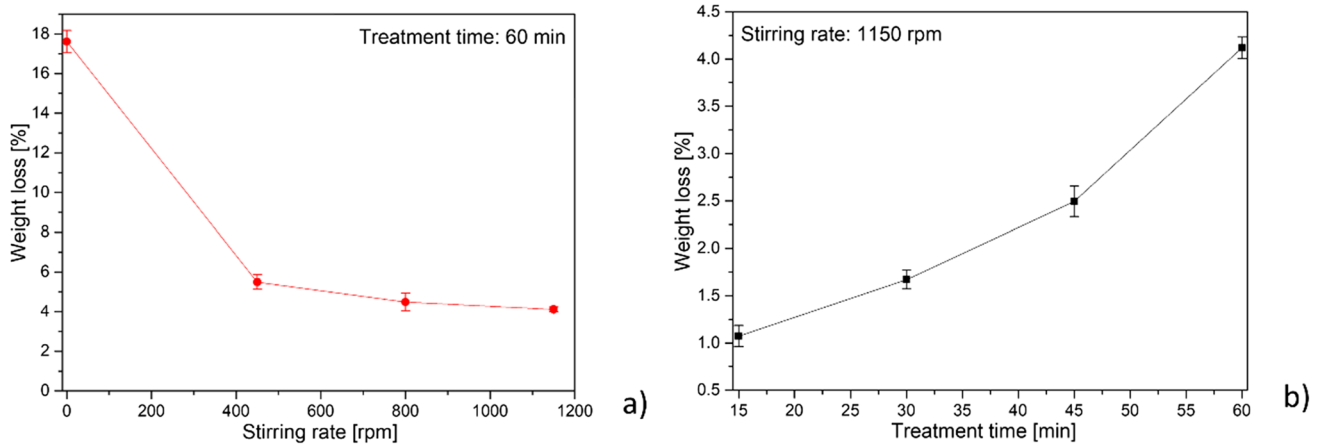
Fig. 9 Measurements of material loss during the EP process by varying **a** the agitation rate of the solution at a fixed time and **b** the treatment time at a fixed stirring rate

Fig. 10 Pictures of dog-bone samples **a** before and **b** after the EP treatment ($\Phi_1 = 35$ mm, rpm = 1150, treatment time = 60 min, room temperature, potential = 25 V)

The mean lifetime of treated and as-built samples is 164779 and 46,515 cycles, respectively. The mean lifetime of treated samples was 250% longer than the mean lifetime of as-built samples. The means of the Z_EP and Z_as-built log-normal distribution are 5.1729 and 4.6550, respectively. In order to verify that the two distributions really have two statistically different means, the Student t-test was performed. The null hypothesis is that the means reported in Table 4 are the same. The independent t-test, with a 95% confidence interval, demonstrated that the two means are significantly different, t(6) = −4.15744, p = 0.005961. Based on these considerations, the fatigue behaviour of EP samples is significantly better than as-built samples.

In Fig. 11a, the cycles to failure of the electropolished and the as-built samples are plotted with the respective probability density functions by adopting the lognormal distribution given in Eq. 1. It is pointed out that at lower stress levels not investigated in this paper, the improved fatigue behaviour of the EP specimens with respect to the as-built is expected to

**Table 4** Summary of fatigue testing results at 378 MPa

Sample ID	Cycles to failure	Mean (μ)	SD (σ)
Z1_as-built	53,527	4.6550	0.12451
Z2_as-built	43,917		
Z3_as-built	30,523		
Z4_as-built	58,096		
Z1_EP	124,064	5.1729	0.21579
Z2_EP	95,021		
Z3_EP	138,065		
Z4_EP	301,967		

increase. In fact, it is known in the literature [50] that a better surface finishing has a beneficial effect of lowering the fatigue limit so that, approaching such a strength level, the electropolished specimens might not fail at all or exhibit a much longer fatigue life than the as-built ones. A qualitative example of this trend is shown in Fig. 11b, where a non-linear model [51] was used to interpolate the fatigue results over a wider stress range, assuming equal tensile strength UTS = 1100 MPa and different fatigue limits for the two sets. Based on this interpolation, at 250 MPa, a life of about 5×10^5 cycles is expected for as-built samples, while an average life of more than 1×10^7 cycles is expected for EP treated.

Figure 12a shows the typical fracture surface of the as-built specimens. A layer of satellite dust, i.e. partially melted powders joined to the sample's outer surface [52], which contributes to the roughness, is clearly visible. More than one fatigue crack initiation site can be detected. The dotted red line in the Fig. highlights the main fracture initiation sites. Higher magnification of the fatigue initiation site for the as-built and electropolished samples is shown in Fig. 12b and c, respectively. Compared to the as-built, the EP-treated fracture surface has no satellites and is characterised by a single fatigue crack nucleation site (Fig. 12c).

4 Conclusions

This research activity investigated the effect of the electropolishing treatment using an eco-friendly electrolytic solution on the fatigue properties of Ti6Al4V specimens produced by electron beam melting technology. The eco-friendly electropolishing treatment was initially studied
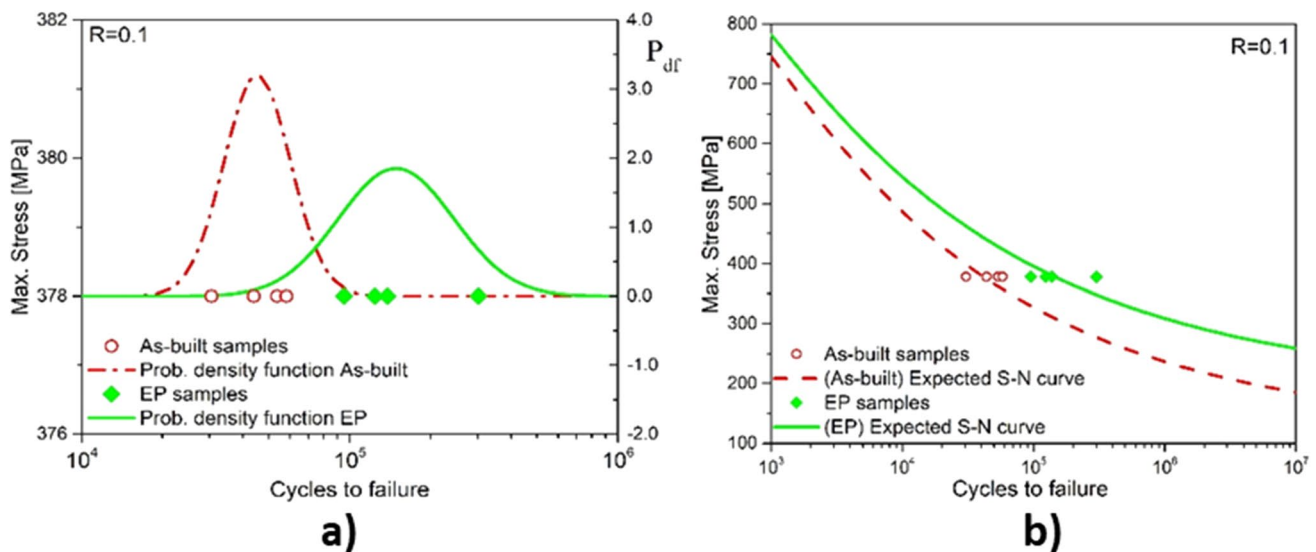
Fig. 11 Comparison of the two experimental data sets in terms of: **a** cycles to failure and probability density function, **b** expected S–N curves interpolating the fatigue results
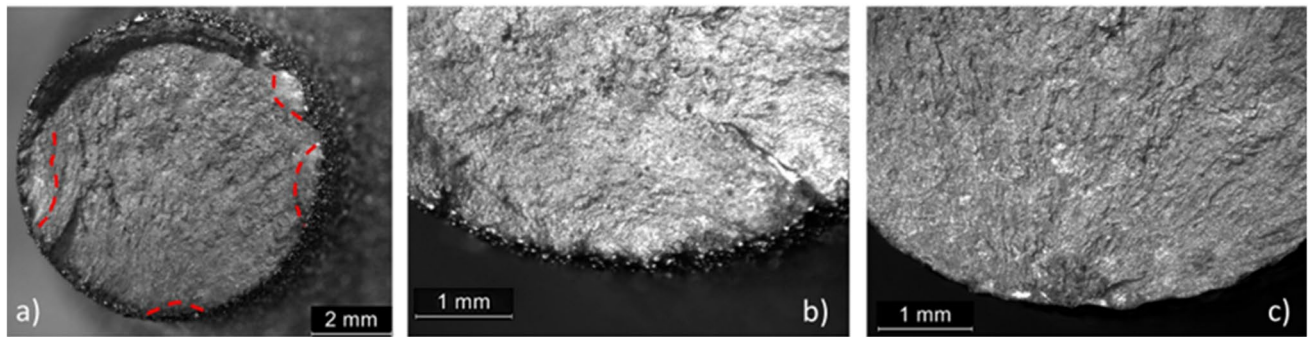
Fig. 12 **a** Fracture surface of the as-built sample with multiple fatigue crack initiation sites; magnified fatigue initiation site in **b** as-built and **c** electropolished sample

using cylindrical specimens. In order to obtain a smoothing of the surface, three parameters have been investigated: the interelectrode distance, the stirring rate and the treatment time. The results were evaluated through topographical, roughness and weight loss measurements. The best condition obtained with cylindrical samples was adopted to electropolish the dog-bone samples, on which a comparative fatigue analysis was carried out. Based on the outcomes presented and discussed in the previous sections, the following conclusions can be drawn:

- The proposed eco-friendly electrochemical treatment was proved to be a feasible process to reduce the roughness of EBM Ti6Al4V printed parts;

- A proper cathode geometry allowed a more uniform treatment, and an interelectrode distance of 3.5 cm was enough to have beneficial effects on the roughness;

- A high stirring rate improves the roughness reduction. The best result was reached when the solution stirring rate was set to 1150 rpm, as also proved by the weight loss measurements;

- With the increase in the treatment time, the surface of the specimens was proved to be smoother, with more rounded and less sharp peaks. However, the results proved that the minimum time to obtain a roughness reduction of 50% is 15 min, while the treatment duration of 60 min allowed to obtain a roughness reduction of about 64%, with a relatively low weight loss of 4.2%;

- The fatigue analysis showed that the mean lifetime of treated samples is 250% longer than the mean lifetime of as-built samples under the same stress conditions ($S_{max} = 378$ MPa; $R = 0.1$). The EP-treated ones had no partially melted particles attached to the surface, and only a single fatigue crack nucleation site was detected. This proved the effectiveness of the eco-friendly EP treatment on fatigue properties of EBM Ti6Al4V printed parts.

Declarations

Ethics approval The manuscript is not submitted to other journals for simultaneous consideration.

Consent to participate Not applicable.

Consent for publication Not applicable.

Conflict of interest The authors declare no competing interests.

References

1. Kekana N, Shongwe MB, Mpofu K, Muvunzi R (2022) A review on factors influencing mechanical properties of AlSi12 alloy processed by selective laser melting. Int J Adv Manuf Technol

121:4313–4323. https://doi.org/10.1007/S00170-022-09582-6/FIGURES/6

2. Rizza G, Galati M, Iuliano L (2022) A phase-field study of neck growth in electron beam powder bed fusion (EB-PBF) process of Ti6Al4V powders under different processing conditions. Int J Adv Manuf Technol 123:855–873. https://doi.org/10.1007/S00170-022-10204-4/FIGURES/5

3. Murr LE, Gaytan SM, Ramirez DA et al (2012) Metal fabrication by additive manufacturing using laser and electron beam melting technologies. J Mater Sci Technol 28:1–14. https://doi.org/10.1016/S1005-0302(12)60016-4

4. Liu S, Shin YC (2019) Additive manufacturing of Ti6Al4V alloy a review. Mater Des 164:107552. https://doi.org/10.1016/J.MATDES.2018.107552

5. Guo N, Leu MC (2013) Additive manufacturing: technology, applications and research needs. Front Mech Eng 83(8):215–243. https://doi.org/10.1007/S11465-013-0248-8

6. Zhao X, Li Q, Xiao M, He Z (2022) Defect detection of 3D printing surface based on geometric local domain features. Int J Adv Manuf Technol 125:183–194. https://doi.org/10.1007/S00170-022-10662-W/TABLES/3

7. HemmasianEttefagh A, Zeng C, Guo S, Raush J (2019) Corrosion behavior of additively manufactured Ti-6Al-4V parts and the effect of post annealing. Addit Manuf 28:252–258. https://doi.org/10.1016/J.ADDMA.2019.05.011

8. Lewandowski JJ, Seifi M (2016) Metal additive manufacturing: a review of mechanical properties. Annu Rev Mater Res 46:151–186. https://doi.org/10.1146/ANNUREV-MATSCI-070115-032024

9. Khairallah SA, Anderson AT, Rubenchik A, King WE (2016) Laser powder-bed fusion additive manufacturing: physics of complex melt flow and formation mechanisms of pores, spatter, and denudation zones. Acta Mater 108:36–45. https://doi.org/10.1016/J.ACTAMAT.2016.02.014

10. Gong H, Rafi K, Gu H et al (2015) Influence of defects on mechanical properties of Ti–6Al–4 V components produced by selective laser melting and electron beam melting. Mater Des 86:545–554. https://doi.org/10.1016/J.MATDES.2015.07.147

11. Franchitti S, Pirozzi C, Borrelli R (2020) Influence of hot isostatic pressing and surface finish on the mechanical behaviour of Ti6Al4V processed by electron beam melting. Fatigue Fract Eng Mater Struct 43:2828–2841. https://doi.org/10.1111/FFE.13295

12. Hu YN, Wu SC, Withers PJ et al (2020) The effect of manufacturing defects on the fatigue life of selective laser melted Ti-6Al-4V structures. Mater Des 192:108708. https://doi.org/10.1016/J.MATDES.2020.108708

13. Fitzmire M, Hejripour F, Molaei R, Asadi E (2023) On the influence of in situ powder bed density variations on defect characteristics and fatigue performance of additively manufactured Ti–6Al–4 V components. Int J Adv Manuf Technol 124:919–934. https://doi.org/10.1007/S00170-022-10545-0/FIGURES/14

14. Serrano-Munoz I, Buffiere JY, Verdu C et al (2016) Influence of surface and internal casting defects on the fatigue behaviour of A357–T6 cast aluminium alloy. Int J Fatigue 82:361–370. https://doi.org/10.1016/J.IJFATIGUE.2015.07.032

15. Rotella A, Nadot Y, Piellard M et al (2020) Influence of defect morphology and position on the fatigue limit of cast Al alloy: 3D characterization by X-ray microtomography of natural and artificial defects. Mater Sci Eng A 785:139347. https://doi.org/10.1016/J.MSEA.2020.139347

16. Fayazfar H, Sharifi J, Keshavarz MK, Ansari M (2023) An overview of surface roughness enhancement of additively manufactured metal parts: a path towards removing the post-print bottleneck for complex geometries. Int J Adv Manuf Technol 125:1061–1113. https://doi.org/10.1007/s00170-023-10814-6

17. Uzan NE, Ramati S, Shneck R et al (2018) On the effect of shot-peening on fatigue resistance of AlSi10Mg specimens fabricated by additive manufacturing using selective laser melting (AM-SLM). Addit Manuf 21:458–464. https://doi.org/10.1016/J.ADDMA.2018.03.030

18. Zhang Y, Li J, Che S et al (2019) Chemical leveling mechanism and oxide film properties of additively manufactured Ti–6Al–4V alloy. J Mater Sci 54:13753–13766. https://doi.org/10.1007/S10853-019-03855-4/TABLES/4

19. Dillard J, Grizzle A, Demisse W et al (2022) Alternating chempolishing and electropolishing for interior and exterior surface finishing of additively manufactured (AM) metal components. Int J Adv Manuf Technol 121:8159–8170. https://doi.org/10.1007/S00170-022-09857-Y/FIGURES/8

20. Mathieu JB, Mathieu HJ, Landolt D (1978) Electropolishing of titanium in perchloric acid-acetic acid solution: I. Auger electron spectroscopy study of anodic films. J Electrochem Soc 125:1039–1043. https://doi.org/10.1149/1.2131617/XML

21. Tyagi P, Brent D, Saunders T et al (2020) Roughness reduction of additively manufactured steel by electropolishing. Int J Adv Manuf Technol 106:1337–1344. https://doi.org/10.1007/S00170-019-04720-Z/FIGURES/6

22. Tajima K, Hironaka M, Chen KK et al (2008) Electropolishing of CP titanium and its alloys in an alcoholic solution-based electrolyte. Dent Mater J 27:258–265. https://doi.org/10.4012/DMJ.27.258

23. Kim D, Son K, Sung D et al (2015) Effect of added ethanol in ethylene glycol–NaCl electrolyte on titanium electropolishing. Corros Sci 98:494–499. https://doi.org/10.1016/J.CORSCI.2015.05.057

24. Acquesta A, Monetta T (2021) The electropolishing of additively manufactured parts in titanium: state of the art. Adv Eng Mater 23:2100545. https://doi.org/10.1002/ADEM.202100545

25. Urlea V, Brailovski V (2017) Electropolishing and electropolishing-related allowances for powder bed selectively laser-melted Ti-6Al-4V alloy components. J Mater Process Technol 242:1–11. https://doi.org/10.1016/J.JMATPROTEC.2016.11.014

26. Benedetti M, Torresani E, Leoni M et al (2017) The effect of post-sintering treatments on the fatigue and biological behavior of Ti-6Al-4V ELI parts made by selective laser melting. J Mech Behav Biomed Mater 71:295–306. https://doi.org/10.1016/J.JMBBM.2017.03.024

27. Wu YC, Kuo CN, Chung YC et al (2019) Effects of electropolishing on mechanical properties and bio-corrosion of Ti6Al4V fabricated by electron beam melting additive manufacturing. Mater 12:1466. https://doi.org/10.3390/MA12091466

28. Pyka G, Burakowski A, Kerckhofs G et al (2012) Surface modification of Ti6Al4V open porous structures produced by additive manufacturing. Adv Eng Mater 14:363–370. https://doi.org/10.1002/ADEM.201100344

29. Neira Arce A (2012) Thermal modeling and simulation of electron beam melting for rapid prototyping on Ti6Al4V alloys

30. Standard test methods for flow rate of metal powders using the hall flowmeter funnel. https://www.astm.org/standards/b213. Accessed 21 Oct 2022

31. Standard Test method for apparent density of free-flowing metal powders using the hall flowmeter funnel. https://www.astm.org/b0212-21.html. Accessed 21 Oct 2022

32. Körner C (2016) Additive manufacturing of metallic components by selective electron beam melting-a review FULL CRITICAL REVIEW Additive manufacturing of metallic components by selective electron beam melting-a review. https://doi.org/10.1080/09506608.2016.1176289

33. Borrelli R, Franchitti S, Pirozzi C et al (2020) Ti6Al4V parts produced by electron beam melting: analysis of dimensional accuracy and surface roughness. J Adv Manuf Syst 19:107–130. https://doi.org/10.1142/S0219686720500067

34. Kim SH, Choi SG, Choi WK, Lee ES (2016) A study of the improvement surface roughness and optimum machining characteristic of L-shaped tube STS 316L by electropolishing. Int J Adv Manuf Technol 85:2313–2324. https://doi.org/10.1007/S00170-015-8041-Y/METRICS

35. Lee ES (2011) Shin TH (2011) An evaluation of the machinability of nitinol shape memory alloy by electrochemical polishing. J Mech Sci Technol 254(25):963–969. https://doi.org/10.1007/S12206-011-0209-2

36. Mathieu JB, Landolt D (1978) Electropolishing of titanium in perchloric acid-acetic acid solution: II. Polarization behavior and stoichiometry. J Electrochem Soc 125:1044–1049. https://doi.org/10.1149/1.2131618/XML

37. Piotrowski O, Madore C, Landolt D (1998) Electropolishing of titanium and titanium alloys in perchlorate-free electrolytes. Plat Surf Finish 85:115–119

38. Łyczkowska-Widłak E, Lochyński P, Nawrat G (2020) Electrochemical polishing of austenitic stainless steels. Mater 13:2557. https://doi.org/10.3390/MA13112557

39. Dong G, Marleau-Finley J, Zhao YF (2019) Investigation of electrochemical post-processing procedure for Ti-6Al-4V lattice structure manufactured by direct metal laser sintering (DMLS). Int J Adv Manuf Technol 104:3401–3417. https://doi.org/10.1007/S00170-019-03996-5/FIGURES/16

40. ISO - ISO 16610–1:2015 - Geometrical product specifications (GPS) — filtration — Part 1: overview and basic concepts. https://www.iso.org/standard/61375.html. Accessed 21 Oct 2022

41. ISO - ISO 25178–2:2012 - Geometrical product specifications (GPS) — surface texture: areal — Part 2: Terms, definitions and surface texture parameters. https://www.iso.org/standard/42785.html. Accessed 21 Oct 2022

42. Triantaphyllou A, Giusca CL, Macaulay GD et al (2015) Surface texture measurement for additive manufacturing. Surf Topogr Metrol Prop 3:024002. https://doi.org/10.1088/2051-672X/3/2/024002

43. Hou N, Wang M, Zhang Y et al (2021) Insights into the fatigue property of titanium alloy Ti-6Al-4V in aero-engine from the subsurface damages induced by milling: state of the art. Int J Adv Manuf Technol 113:1229–1235. https://doi.org/10.1007/S00170-021-06749-5/FIGURES/5

44. Standard practice for statistical analysis of linear or linearized stress-life (S-N) and Strain-Life (ε-N) Fatigue Data. https://www.astm.org/standards/e739. Accessed 21 Oct 2022

45. Standard practice for conducting force controlled constant amplitude axial fatigue tests of metallic materials. https://www.astm.org/e0466-21.html. Accessed 21 Oct 2022

46. Jacquet PA (1956) Electrolytic and chemical polishing. Metall Rev 1:157–238. https://doi.org/10.1179/MTLR.1956.1.1.157

47. Fushimi K, Habazaki H (2008) Anodic dissolution of titanium in NaCl-containing ethylene glycol. Electrochim Acta 53:3371–3376. https://doi.org/10.1016/J.ELECTACTA.2007.11.074

48. Nesli S, Yilmaz O (2021) Surface characteristics of laser polished Ti-6Al-4V parts produced by electron beam melting additive manufacturing process. Int J Adv Manuf Technol 114:271–289. https://doi.org/10.1007/S00170-021-06861-6/FIGURES/23

49. Ju BF, Chen YL, Fu M et al (2009) Systematic study of electropolishing technique for improving the quality and production reproducibility of tungsten STM probe. Sens Actuators A Phys 155:136–144. https://doi.org/10.1016/J.SNA.2009.08.013

50. McKelvey SA, Fatemi A (2012) Surface finish effect on fatigue behavior of forged steel. Int J Fatigue 36:130–145. https://doi.org/10.1016/J.IJFATIGUE.2011.08.008

51. Esposito L, Bertocco A, Cricrì G (2019) Rosiello V (2019) Welding-repair effect on F357–T6 aluminum castings: analysis of fatigue life. Int J Adv Manuf Technol 1029(102):3699–3706. https://doi.org/10.1007/S00170-019-03436-4

52. Bertocco A, Iannitti G, Caraviello A, Esposito L (2022) Lattice structures in stainless steel 17–4PH manufactured via selective laser melting (SLM) process: dimensional accuracy, satellites formation, compressive response and printing parameters optimization. Int J Adv Manuf Technol 120:4935–4949. https://doi.org/10.1007/S00170-022-08946-2/FIGURES/19